Micropolar Fluid Flow over a Frustum of Cone Subjected to Convective Boundary Condition: Darcy–Forchheimer Model

T. Pradeepa and Ch. RamReddy

Abstract This paper emphasizes the Soret and viscous dissipation effects on mixed convective flow of an incompressible micropolar fluid over a vertical frustum of a cone embedded in a non-Darcy porous medium subject to convective boundary condition. The similarity solution does not attain for this complicated fluid flow problem. Using non-similarity transformations, the governing boundary layer equations are converted into a set of non-dimensional partial differential equations. Prior to being these non-similarity equations are linearized by quasilinearization method and solved by the Chebyshev spectral collocation method. Several features emerging from these parameters, namely micropolar, viscous dissipation, Biot, and Soret numbers on physical quantities of the flow, are explored in detail.

Keywords Convective boundary condition · Truncated cone · Micropolar fluid · Non-Darcy porous medium · Spectral quasi-linearization method

1 Introduction

The convective heat and mass transfer analysis in Darcy and/or non-Darcy porous medium have received significant attention from theoretical as well as practical point of view, owing to its applications mentioned in many areas such as geothermal and petroleum resources, enhanced oil recovery, drying of porous solids, cooling of nuclear reactors, thermal insulation, solid matrix heat exchanges, and other practical interesting designs. The non-Darcy (Forchheimer model) is a modification of classical Darcy model by incorporating the inertial effects (i.e., addition of a squared term

T. Pradeepa (✉)
Department of Mathematics, Telangana Social Welfare Residential Degree College, Mahabubabad, Telangana State, India
e-mail: pradeepa.23@gmail.com

Ch. RamReddy
Department of Mathematics, National Institute of Technology Warangal, Warangal 506004, India
e-mail: chramreddy@nitw.ac.in; chittetiram@gmail.com

S. S. Ray et al. (eds.), *Applied Analysis, Computation and Mathematical Modelling in Engineering*, Lecture Notes in Electrical Engineering 897,
https://doi.org/10.1007/978-981-19-1824-7_9

of velocity) in the momentum equation. The literary work on the convective flow due to buoyancy and external forces in a non-Darcy (Forchheimer model) porous medium has been provided by [1–3] (for more details, see the references cited therein).

Micropolar fluids are the subclass of micro-fluids initiated by Eringen [4]. Compared to the classical Newtonian fluids, the flow motion of micropolar fluids distinguishes by two supplementary variables, i.e., the spin vector, responsible for the micro-rotations, and the micro-inertia tensor describes the distribution of atoms and molecules inside the fluid elements in addition to the velocity vector. Thus, micropolar fluids are able to delineate the rheological behavior of animal blood, drug suspension in pharmacology, liquid crystal, colloidal fluids, plasma, etc. The comprehensive review of micropolar fluid mechanics has been reported by [5–8]. The locally produced thermal energy due to viscous stress mechanism, commonly known as viscous dissipation, influences forced, mixed and free convective flows for fluid saturated porous medium and clear viscous fluids. It has unavoidable role in the convective transport mechanism when the fluid flow field is at low temperature or in high gravitational force field or of extreme size. Extensive research can be found in the literature to study the viscous dissipation effect on micropolar fluid flow over different geometries. To mention a few [9–12].

From literature survey, it is found that this type of flow study over truncated cone is applicable in polymer industry, processing of edible items or slurries, melted plastics at industrial level due to involvement of cone-shaped bodies in these areas. However, no literature is observed regarding the mixed convective transport in a Darcy/non-Darcy porous medium saturated by Newtonian/non-Newtonian fluids with truncated cone as a geometry. Yih [13] examined the numerical solution for the natural convection flow from the vertical truncated cone through saturated porous medium using Keller box method. The buoyancy-driven convective flow of a nanofluid from the frustum of a cone embedded in a porous medium by taking thermophoresis and Brownian motion effects has been elaborated by Cheng [14]. Postelnicu [15] considered the local non-similarity solution for the micropolar fluid flow due to buoyancy forces subjected to flux condition. Patrulescu et al. [16] discussed the mixed convection boundary layer flow of a fluid with three nanoparticles through a truncated cone and observed that existence of dual solution for flow reversal.

The main intention of this study is to understand the mixed convective transport over a convectively heated truncated cone embedded in a non-Darcy porous medium saturated by an incompressible micropolar fluid. In addition, viscous dissipation and thermal diffusion effects are taken into consideration. The similarity solution does not obtain for the intricate flow situation, and hence, the non-similarity solution is attained by using spectral quasilinearization method and the usefulness of pertinent parameters discussed through graphical representations.

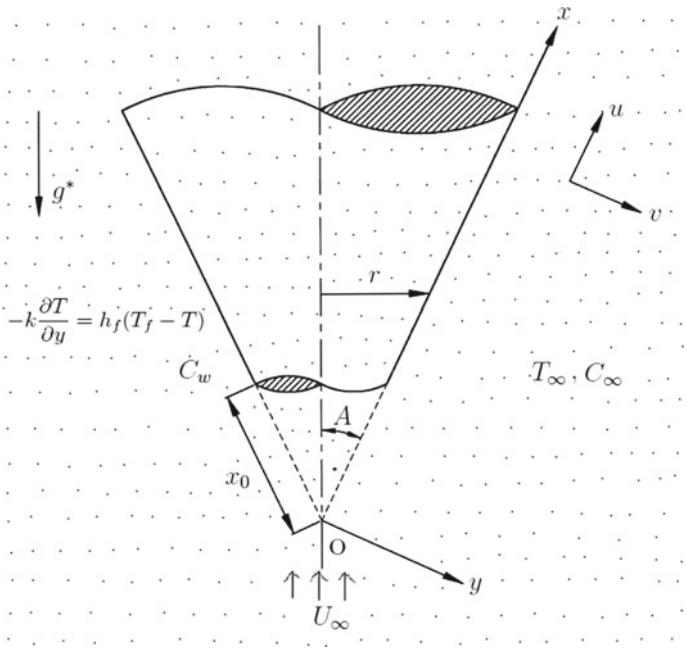

Fig. 1 Physical model and coordinates for a truncated cone

2 Mathematical Analysis

The steady, 2D, laminar mixed convective flow of a micropolar fluid over a truncated cone in a non-Darcy porous medium is considered. The porous medium is considered to be isotropic and homogeneous. The solutal concentration is taken to be constant and is given by C_w. The outer flow velocity is in the form of U_∞. At the ambient media, the temperature and concentration are T_∞ and C_∞, respectively. By convection, the surface of the vertical frustum of a cone is either cooled or heated from a fluid of temperature T_f with $T_f < T_\infty$ relating to a cooled surface and $T_f > T_\infty$ relating to a heated surface. The physical geometry of the problem is shown in Fig. (1). The coordinate system is such that the x-coordinate is taken along the vertical frustum of a cone and y-coordinate is measured normal to it.

By employing Boussinesq approximations, the governing equations for incompressible micropolar fluid using Darcy–Forchheimer model [17] are given by

$$\frac{\partial(u\,r)}{\partial x} + \frac{\partial(v\,r)}{\partial y} = 0 \tag{1}$$

$$\frac{\rho}{\epsilon^2}\left(u\frac{\partial u}{\partial x} + v\frac{\partial u}{\partial y}\right) = \left(\frac{\mu+\kappa}{\epsilon}\right)\frac{\partial^2 u}{\partial y^2} + \kappa\frac{\partial \omega}{\partial y} - \frac{\mu}{K_p}(u - U_\infty) - \frac{\rho\, b}{K_p}\left(u^2 - U_\infty^2\right) \tag{2}$$

$$+ \rho g^* \left(\beta_T (T - T_\infty) + \beta_C (C - C_\infty)\right) \cos A$$

$$\frac{\rho j}{\epsilon}\left(u\frac{\partial \omega}{\partial x} + v\frac{\partial \omega}{\partial y}\right) = \gamma \frac{\partial^2 \omega}{\partial y^2} - \kappa\left(2\omega + \frac{1}{\epsilon}\frac{\partial u}{\partial y}\right) \tag{3}$$

$$u\frac{\partial T}{\partial x} + v\frac{\partial T}{\partial y} = \alpha \frac{\partial^2 T}{\partial y^2} + \left(\frac{\mu + \kappa}{\rho C_p}\right)\left(\frac{\partial u}{\partial y}\right)^2 \tag{4}$$

$$u\frac{\partial C}{\partial x} + v\frac{\partial C}{\partial y} = D\frac{\partial^2 C}{\partial y^2} + \frac{D K_T}{T_m}\frac{\partial^2 T}{\partial y^2} \tag{5}$$

where u and v denote the components of velocity in x and y directions, respectively, T represents the temperature, ω is the microrotation component, b indicates the Forchheimer constant, g^* represents the acceleration due to gravity, γ specifies spin-gradient viscosity, r is the truncated cone radius, ρ is the fluid density, C is the concentration, x_0 represents the frustum of a cone leading edge distance measured from the origin, C_p is the specific heat, j represents the micro-inertia density, ϵ indicates porosity, μ represents dynamic coefficient of viscosity, K_T specifies thermal diffusion ratio, β_T represents coefficient of thermal expansion, D represents the solutal diffusivity, κ represents the vortex viscosity, K_p indicates permeability, β_C is the coefficient of solutal expansion, T_m is mean fluid temperature, and α denotes thermal diffusivity. Further, followed the work of several authors by presuming that $\gamma = \left(\mu + \frac{\kappa}{2}\right) j$ [18].

The boundary conditions are

$$u = 0, \quad v = 0, \quad \omega = -n\frac{\partial u}{\partial y}, \quad -k\frac{\partial T}{\partial y} = h_f (T_f - T), \quad C = C_w \quad \text{at} \quad y = 0 \tag{6a}$$

$$u = U_\infty, \quad \omega = 0, \quad T = T_\infty, \quad C = C_\infty \quad \text{as} \quad y \to \infty \tag{6b}$$

here, the subscripts w and ∞ represent the conditions at the wall and boundary layer outer edge, respectively, n is material constant parameter, k is thermal conductivity of fluid, and h_f indicates the convective heat transfer coefficient.

Now, introduce a stream function ψ as

$$u = \frac{1}{r}\frac{\partial \psi}{\partial y}, \quad v = -\frac{1}{r}\frac{\partial \psi}{\partial x} \tag{7}$$

When the thickness of boundary layer is sufficiently less relative to the local radius of a truncated cone, then the local radius to a point in the boundary layer can be approximated by truncated cone radius:

$$r = xsinA \tag{8}$$

Here, defining the non-similarity transformations in the following form

$$\eta = \frac{y}{\bar{x}} Re_x^{1/2},\ \xi = \frac{\bar{x}}{x_0} = \frac{x - x_0}{x_0},\ \omega = \frac{\nu\, Re_x^{3/2}}{\bar{x}^2}\, g\,(\xi, \eta)\,, \tag{9}$$

$$\psi = r\nu Re_x^{1/2} f\,(\xi, \eta)\,,\ \theta\,(\xi, \eta) = \frac{T - T_\infty}{T_f - T_\infty},\ \phi\,(\xi, \eta) = \frac{C - C_\infty}{C_w - C_\infty}$$

where $\bar{x} = x - x_0$ and $Re_x = \dfrac{U_\infty \bar{x}}{\nu}$ is the local Reynolds number.
Substitute (7) - (9) into (2)- (5), the set of equations reduces to the following form

$$\frac{1}{\epsilon}\left(\frac{1}{1-N}\right) f''' + \frac{1}{\epsilon^2}\left(R + \frac{1}{2}\right) f f'' + \frac{\xi}{Da\, Re_{x_0}}(1 - f') + \xi \frac{Fs}{Da}\left(1 - (f')^2\right) \tag{10}$$

$$+ \left(\frac{N}{1-N}\right) g' + \xi\, \lambda\, (\theta + \mathcal{B}\phi) = \frac{\xi}{\epsilon^2}\left(f' \frac{\partial f'}{\partial \xi} - f'' \frac{\partial f}{\partial \xi}\right)$$

$$\left(\frac{2-N}{2-2N}\right) g'' + \frac{1}{\epsilon}\left(R + \frac{1}{2}\right) f\, g' + \frac{1}{2\epsilon} f'\, g - \xi \left(\frac{N}{1-N}\right)\left(2g + \frac{1}{\epsilon} f''\right) = \frac{\xi}{\epsilon}\left(f' \frac{\partial g}{\partial \xi} - g' \frac{\partial f}{\partial \xi}\right) \tag{11}$$

$$\frac{1}{Pr}\theta'' + \left(R + \frac{1}{2}\right) f\, \theta' + \left(\frac{1}{1-N}\right) \varepsilon\, (f'')^2 = \xi \left(f' \frac{\partial \theta}{\partial \xi} - \theta' \frac{\partial f}{\partial \xi}\right) \tag{12}$$

$$\frac{1}{Sc}\phi'' + \left(R + \frac{1}{2}\right) f\, \phi' + Sr\, \theta'' = \xi \left(f' \frac{\partial \phi}{\partial \xi} - \phi' \frac{\partial f}{\partial \xi}\right) \tag{13}$$

where the primes denote partial derivative with respect to η alone. $N = \left(\dfrac{\kappa}{\mu + \kappa}\right)$ represents the coupling number [19], $Gr = \dfrac{g^* \beta_T (T_f - T_\infty) \bar{x}^3 cosA}{\nu^2}$ denotes the thermal Grashof number, $\varepsilon = \dfrac{U_\infty^2}{C_p (T_f - T_\infty)}$ is the viscous dissipation parameter, $Gc = \dfrac{g^* \beta_C (C_w - C_\infty) \bar{x}^3 cosA}{\nu^2}$ represents the solutal Grashof number, $Fs = \dfrac{b}{x_0}$ represents the Forchheimer number, $Pr = \dfrac{\nu}{\alpha}$ indicates the Prandtl number, $Da = \dfrac{K_p}{x_0^2}$ is the Darcy parameter, $Sr = \dfrac{DK_T (T_f - T_\infty)}{\nu T_m (C_w - C_\infty)}$ is the Soret number, $Sc = \dfrac{\nu}{D}$ is the Schmidt number, $\mathcal{B} = \dfrac{Gc}{Gr}$ is the buoyancy ratio, $\lambda = \dfrac{Gr_{x_0}}{Re_{x_0}^2}$ indicates the mixed

convection parameter and $Re_{x_0} = \dfrac{U_\infty x_0}{\nu}$ is the Reynolds number. Also, notice that $\lambda < 0$, $\lambda = 0$ and $\lambda > 0$ correspond to opposing flow, forced convection flow, and assisting flow, respectively.

The boundary conditions are

$$\left(R + \frac{1}{2}\right) f(\xi,\eta) + \xi \frac{\partial f}{\partial \xi} = 0,\ f'(\xi,\eta) = 0,\ g(\xi,\eta) = -nf''(\xi,\eta), \tag{14a}$$

$$\theta'(\xi,\eta) = -\xi^{1/2} Bi(1 - \theta(\xi,\eta)),\ \phi(\xi,\eta) = 1 \quad at\ \eta = 0,$$

$$f'(\xi,\eta) = 1,\ g(\xi,\eta) = 0,\ \theta(\xi,\eta) = 0,\ \phi(\xi,\eta) = 0 \quad as\,\eta \to \infty. \tag{14b}$$

where $R = \dfrac{\xi}{1+\xi}$, $Bi = \dfrac{h_f\, x_0}{k\, Re_{x_0}^{1/2}}$ represents the Biot number. R becomes zero when $\xi = 0$; hence, the present problem diminishes to mixed convective flow along a vertical plate in a micropolar fluid. As $\xi \to \infty$, $R \to 1$, since $\xi = (x - x_0)/x_0$, ξ becoming large means x is far downstream or cross section of truncated cone radius leading edge is very small.

3 Skin Friction, Wall Couple Stress, Heat and Mass Transfer Coefficients

The wall shear stress and wall couple stress are:

$$\tau_w = \left[(\mu + \kappa)\frac{\partial u}{\partial y} + \kappa\omega\right]_{y=0}, m_w = \gamma\left[\frac{\partial \omega}{\partial y}\right]_{y=0},$$

The heat transfer and mass transfer rates:

$$q_w = -k\left[\frac{\partial T}{\partial y}\right]_{y=0},\ q_m = -D\left[\frac{\partial C}{\partial y}\right]_{y=0}$$

The non-dimensional skin friction $C_f = \dfrac{2\tau_w}{\rho\, U_\infty^2}$, wall couple stress $M_w = \dfrac{m_w}{\rho\, U_\infty^2 x_0}$, the local Nusselt number $Nu_x = \dfrac{q_w \bar{x}}{k(T_f - T_\infty)}$ and local Sherwood number $Sh_x = \dfrac{q_m \bar{x}}{D(C_w - C_\infty)}$ are given by

$$\left.\begin{aligned} C_f Re_x^{1/2} &= 2\left(\frac{1-nN}{1-N}\right) f''(\xi,0), \qquad M_w Re_x = \left(\frac{2-N}{2-2N}\right) g'(\xi,0), \\ \frac{Nu_x}{Re_x^{1/2}} &= -\theta'(\xi,0), \qquad \frac{Sh_x}{Re_x^{1/2}} = -\phi'(\xi,0). \end{aligned}\right\} \tag{15}$$

where $Re_x = \dfrac{U_\infty \bar{x}}{\nu}$ is the local Reynold's number.

4 Solution of the Problem

The non-homogeneous and nonlinear coupled partial differential equations(PDE's) (10)–(13) along with boundary conditions (14) have been solved numerically by spectral quasi-linearization method (SQLM) [20, 21]. Essentially, quasilinearization technique is the generalized Newton–Raphson method initiated by Bellman and Kalaba [22] for solving the functional equations. By applying quasilinearization procedure to Eqs. (10)–(13), the resultant equations are:

$$\frac{1}{\epsilon}\left(\frac{1}{1-N}\right) f'''_{r+1} + a_{1,r} f''_{r+1} + \left(\frac{N}{1-N}\right) g'_{r+1} + a_{2,r} f'_{r+1} + a_{3,r} f_{r+1} + a_{4,r} \tag{16}$$

$$+\xi\,\lambda\,\theta_{r+1} + \xi\,\lambda\,\mathcal{B}\,\phi_{r+1} - a_{5,r}\frac{\partial f'_{r+1}}{\partial \xi} - a_{6,r}\frac{\partial f_{r+1}}{\partial \xi} = 0,$$

$$\left(\frac{2-N}{2-2N}\right) g''_{r+1} - \frac{\xi}{\epsilon}\left(\frac{N}{1-N}\right) f''_{r+1} + b_{1,r}\, g'_{r+1} + b_{2,r}\, g_{r+1} + b_{3,r} f'_{r+1} \tag{17}$$

$$+b_{4,r} f_{r+1} + b_{5,r} - b_{6,r}\frac{\partial g_{r+1}}{\partial \xi} - b_{7,r}\frac{\partial f_{r+1}}{\partial \xi} = 0,$$

$$\frac{1}{Pr}\,\theta''_{r+1} + c_{1,r}\,\theta'_{r+1} + c_{2,r} f''_{r+1} + c_{3,r} f'_{r+1} + c_{4,r} f_{r+1} + c_{5,r} - c_{6,r}\frac{\partial \theta_{r+1}}{\partial \xi} - c_{7,r}\frac{\partial f_{r+1}}{\partial \xi} = 0, \tag{18}$$

$$\frac{1}{Sc}\,\phi''_{r+1} + d_{1,r}\,\phi'_{r+1} + Sr\,\theta''_{r+1} + d_{2,r} f'_{r+1} + d_{3,r} f_{r+1} + d_{4,r} - d_{5,r}\frac{\partial \phi_{r+1}}{\partial \xi} - d_{6,r}\frac{\partial f_{r+1}}{\partial \xi} = 0, \tag{19}$$

where

$$a_{1,r} = \frac{1}{\epsilon^2}\left(R + \frac{1}{2}\right) f_r + \frac{\xi}{\epsilon^2}\frac{\partial f_r}{\partial \xi};\; a_{2,r} = \frac{-\xi}{Da\, Re_{x_0}} - \xi\frac{2Fs}{Da} f'_r - \frac{\xi}{\epsilon^2}\frac{\partial f'_r}{\partial \xi};\; a_{3,r} = \frac{1}{\epsilon^2}\left(R + \frac{1}{2}\right) f''_r;$$

$$a_{4,r} = \frac{-1}{\epsilon^2}\left(R + \frac{1}{2}\right) f_r f''_r + \frac{\xi}{Da\, Re_{x_0}} + \xi\,\frac{Fs}{Da} + \xi\frac{Fs}{Da} f'^2_r + \frac{\xi}{\epsilon^2} f'_r \frac{\partial f'_r}{\partial \xi} - \frac{\xi}{\epsilon^2} f''_r \frac{\partial f_r}{\partial \xi};\; a_{5,r} = \frac{\xi}{\epsilon^2} f'_r;\; a_{6,r} = \frac{-\xi}{\epsilon^2} f''_r;$$

$$b_{1,r} = \frac{1}{\epsilon}\left(R+\frac{1}{2}\right)f_r + \frac{\xi}{\epsilon}\frac{\partial f_r}{\partial \xi};\ b_{2,r} = \frac{1}{2\epsilon}f_r' - 2\xi\left(\frac{N}{1-N}\right);\ b_{3,r} = \frac{1}{2\epsilon}g_r - \frac{\xi}{\epsilon}\frac{\partial g_r}{\partial \xi};$$

$$b_{4,r} = \frac{1}{\epsilon}\left(R+\frac{1}{2}\right)g_r';\ b_{5,r} = \frac{-1}{\epsilon}\left(R+\frac{1}{2}\right)f_r\, g_r' - \frac{1}{2\epsilon}f_r'\, g_r + \frac{\xi}{\epsilon}f_r'\frac{\partial g_r}{\partial \xi} - \frac{\xi}{\epsilon}g_r'\frac{\partial f_r}{\partial \xi};\ b_{6,r} = \frac{\xi}{\epsilon}f_r';\ b_{7,r} = \frac{-\xi}{\epsilon}g_r';$$

$$c_{1,r} = \left(R+\frac{1}{2}\right)f_r + \xi\frac{\partial f_r}{\partial \xi};\ c_{2,r} = 2\varepsilon\left(\frac{1}{1-N}\right)f_r'';\ c_{3,r} = -\xi\frac{\partial \theta_r}{\partial \xi};\ c_{4,r} = \left(R+\frac{1}{2}\right)\theta_r';\ c_{7,r} = -\xi\theta_r';$$

$$c_{5,r} = -\left(R+\frac{1}{2}\right)f_r\,\theta_r' - \varepsilon\left(\frac{1}{1-N}\right)f_r''^2 + \xi f_r'\frac{\partial \theta_r}{\partial \xi} - \xi\theta_r'\frac{\partial f_r}{\partial \xi};\ c_{6,r} = \xi f_r';$$

$$d_{1,r} = \left(R+\frac{1}{2}\right)f_r + \xi\frac{\partial f_r}{\partial \xi};\ d_{2,r} = -\xi\frac{\partial \phi_r}{\partial \xi};\ d_{3,r} = \left(R+\frac{1}{2}\right)\phi_r';\ d_{6,r} = -\xi\phi_r';$$

$$d_{4,r} = -\left(R+\frac{1}{2}\right)f_r\,\phi_r' + \xi f_r'\frac{\partial \phi_r}{\partial \xi} - \xi\phi_r'\frac{\partial f_r}{\partial \xi};\ d_{5,r} = \xi f_r';$$

Discretize Eqs. (16) to (19) using the spectral collocation method (i.e., Chebyshev) [23, 24] in the direction of η, and the implicit finite difference method is applied in ξ direction. The collocation points on (η, ξ) are interpreted as

$$\tau_j = \cos\left(\frac{\pi j}{N_x}\right),\quad \xi^n = n\Delta\xi \qquad j = 0, 1, 2, \ldots, N_x,\ \ n = 0, 1, 2, \ldots, N_t \tag{20}$$

where N_x+1 indicates the number of collocation points in η direction, $\Delta\xi$ is the spacing, and $N_t + 1$ is total number of collocation points in the direction of ξ.

The primitive concept beyond this method is the representation of a derivative matrix D, used to approximate the derivative coefficients $f(\eta)$ of unknown variables at the grid points as the matrix vector product:

$$\frac{df}{d\eta} = \sum_{k=0}^{N_x} D_{lk} f(\tau_k) = \mathbf{DF},\ \ l = 0, 1, \ldots, N_x, \tag{21}$$

Here, the vector function at the collocation(grid) point is represented by $\mathbf{F} = [f(\tau_0), f(\tau_1), f(\tau_2) \ldots, f(\tau_{N_x})]^T$; similarly, the vector functions corresponding to ϕ, g, and θ are termed as Φ, $\mathbf{G}$, and Θ, respectively. The derivative is scaled as $\mathbf{D} = \dfrac{2\mathcal{D}}{L}$; here, D represents derivative with respect to η. The derivatives of higher order are expressed as exponents of $\mathbf{D}$,

$$f^{(m)} = \mathbf{D}^m\mathbf{F},\ g^{(m)} = \mathbf{D}^m\mathbf{G},\ \theta^{(m)} = \mathbf{D}^m\Theta,\ \phi^{(m)} = \mathbf{D}^m\Phi. \tag{22}$$

where $\mathbf{D}$ indicates the Chebyshev derivative matrix of size $(N_x + 1) \times (N_x + 1)$, and m is the order of derivative. With centering about a midpoint halfway between ξ^n and ξ^{n+1} finite difference scheme is imposed, this midpoint is elucidated as $\xi^{n+\frac{1}{2}} = \left(\xi^{n+1} + \xi^n\right)/2$. Applying $\xi^{n+\frac{1}{2}}$ to any other function, for instance $f(\xi, \eta)$ and its related derivative obtained as

$$f(\xi^{n+\frac{1}{2}}, \eta_j) = f_j^{n+\frac{1}{2}} = \frac{f_j^{n+1} + f_j^n}{2} \tag{23}$$

$$\left(\frac{\partial f}{\partial \xi}\right)^{n+\frac{1}{2}} = \frac{f_j^{n+1} - f_j^n}{\Delta\xi} \tag{24}$$

Applying finite difference in ξ and spectral methods on Eqs. (16)–(19) gives

$$\begin{bmatrix} A_{11} & A_{12} & A_{13} & A_{14} \\ A_{21} & A_{22} & A_{23} & A_{24} \\ A_{31} & A_{32} & A_{33} & A_{34} \\ A_{41} & A_{42} & A_{43} & A_{44} \end{bmatrix} \begin{bmatrix} F_{r+1}^{n+1} \\ G_{r+1}^{n+1} \\ \Theta_{r+1}^{n+1} \\ \Phi_{r+1}^{n+1} \end{bmatrix} = \begin{bmatrix} B_{11} & B_{12} & B_{13} & B_{14} \\ B_{21} & B_{22} & B_{23} & B_{24} \\ B_{31} & B_{32} & B_{33} & B_{34} \\ B_{41} & B_{42} & B_{43} & B_{44} \end{bmatrix} \begin{bmatrix} F_{r+1}^{n} \\ G_{r+1}^{n} \\ \Theta_{r+1}^{n} \\ \Phi_{r+1}^{n} \end{bmatrix} + \begin{bmatrix} K_1 \\ K_2 \\ K_3 \\ K_4 \end{bmatrix}$$

where A_{ij}, B_{ij}, $(i, j = 1, 2, 3, 4)$ are $(N_x + 1) \times (N_x + 1)$ matrices and K_i, $(i = 1, 2, 3, 4)$ is $(N_x + 1) \times 1$ vectors defined as

$$A_{11} = \frac{1}{2}\left[\frac{1}{\epsilon}\left(\frac{1}{1-N}\right)\mathbf{D}^3 + a_{1,r}^{n+\frac{1}{2}}\mathbf{D}^2 + a_{2,r}^{n+\frac{1}{2}}\mathbf{D} + a_{3,r}^{n+\frac{1}{2}}\right] - \frac{a_{5,r}^{n+\frac{1}{2}}\mathbf{D}}{\Delta\xi} - \frac{a_{6,r}^{n+\frac{1}{2}}}{\Delta\xi};$$

$$A_{12} = \frac{1}{2}\left[\left(\frac{N}{1-N}\right)\mathbf{D}\right];\ A_{13} = \frac{1}{2}\xi\,\lambda\mathbf{I};\ A_{14} = \frac{1}{2}\xi\,\lambda\mathcal{B}\,\mathbf{I};$$

$$A_{21} = \frac{1}{2}\left[\frac{\xi}{\epsilon}\left(\frac{-N}{1-N}\right)\mathbf{D}^2 + b_{3,r}^{n+\frac{1}{2}}\mathbf{D} + b_{4,r}^{n+\frac{1}{2}}\right] - \frac{b_{7,r}^{n+\frac{1}{2}}}{\Delta\xi};\ A_{24} = \mathbf{0};$$

$$A_{22} = \frac{1}{2}\left[\left(\frac{2-N}{2-2N}\right)\mathbf{D}^2 + b_{1,r}^{n+\frac{1}{2}}\mathbf{D} + b_{2,r}^{n+\frac{1}{2}}\right] - \frac{b_{6,r}^{n+\frac{1}{2}}}{\Delta\xi};\ A_{23} = \mathbf{0};$$

$$A_{31} = \frac{1}{2}\left[c_{2,r}^{n+\frac{1}{2}}\mathbf{D}^2 + c_{3,r}^{n+\frac{1}{2}}\mathbf{D} + c_{4,r}^{n+\frac{1}{2}}\right] - \frac{c_{7,r}^{n+\frac{1}{2}}}{\Delta\xi};\ A_{32} = \mathbf{0};$$

$$A_{33} = \frac{1}{2}\left[\frac{1}{Pr}\mathbf{D}^2 + c_{1,r}^{n+\frac{1}{2}}\mathbf{D}\right] - \frac{c_{6,r}^{n+\frac{1}{2}}}{\Delta\xi};\ A_{34} = \mathbf{0};$$

$$A_{41} = \frac{1}{2}\left[d_{2,r}^{n+\frac{1}{2}}\mathbf{D} + d_{3,r}^{n+\frac{1}{2}}\right] - \frac{d_{6,r}^{n+\frac{1}{2}}}{\Delta\xi};\ A_{42} = \mathbf{0};$$

$$A_{43} = \frac{1}{2}Sr\mathbf{D}^2;\ A_{44} = \frac{1}{2}\left[\frac{1}{Sc}\mathbf{D}^2 + d_{1,r}^{n+\frac{1}{2}}\mathbf{D}\right] - \frac{d_{5,r}^{n+\frac{1}{2}}}{\Delta\xi};$$

$$B_{11} = -\frac{1}{2}\left[\frac{1}{\epsilon}\left(\frac{1}{1-N}\right)\mathbf{D}^3 + a_{1,r}^{n+\frac{1}{2}}\mathbf{D}^2 + a_{2,r}^{n+\frac{1}{2}}\mathbf{D} + a_{3,r}^{n+\frac{1}{2}}\right] - \frac{a_{5,r}^{n+\frac{1}{2}}\mathbf{D}}{\Delta\xi} - \frac{a_{6,r}^{n+\frac{1}{2}}}{\Delta\xi};$$

$$B_{12} = -\frac{1}{2}\left[\left(\frac{N}{1-N}\right)\mathbf{D}\right];\ B_{13} = -\frac{1}{2}\xi\lambda\mathbf{I};\ B_{14} = -\frac{1}{2}\lambda\xi\mathcal{B}\mathbf{I}$$

$$B_{21} = -\frac{1}{2}\left[\frac{\xi}{\epsilon}\left(\frac{-N}{1-N}\right)\mathbf{D}^2 + b_{3,r}^{n+\frac{1}{2}}\mathbf{D} + b_{4,r}^{n+\frac{1}{2}}\right] - \frac{b_{7,r}^{n+\frac{1}{2}}}{\Delta\xi};$$

$$B_{22} = -\frac{1}{2}\left[\left(\frac{2-N}{2-2N}\right)\mathbf{D}^2 + b_{1,r}^{n+\frac{1}{2}}\mathbf{D} + b_{2,r}^{n+\frac{1}{2}}\right] - \frac{b_{6,r}^{n+\frac{1}{2}}}{\Delta\xi};\ B_{23} = \mathbf{0};\ B_{24} = \mathbf{0};$$

$$B_{31} = -\frac{1}{2}\left[c_{2,r}^{n+\frac{1}{2}}\mathbf{D}^2 + c_{3,r}^{n+\frac{1}{2}}\mathbf{D} + c_{4,r}^{n+\frac{1}{2}}\right] - \frac{c_{7,r}^{n+\frac{1}{2}}}{\Delta\xi};\ B_{32} = \mathbf{0};$$

$$B_{33} = -\frac{1}{2}\left[\frac{1}{Pr}\mathbf{D}^2 + c_{1,r}^{n+\frac{1}{2}}\mathbf{D}\right] - \frac{c_{6,r}^{n+\frac{1}{2}}}{\Delta\xi};\ B_{34} = \mathbf{0};$$

$$B_{41} = -\frac{1}{2}\left[d_{2,r}^{n+\frac{1}{2}}\mathbf{D} + d_{3,r}^{n+\frac{1}{2}}\right] - \frac{d_{6,r}^{n+\frac{1}{2}}}{\Delta\xi};\ B_{42} = \mathbf{0};$$

$$B_{43} = -\frac{1}{2}Sr\mathbf{D}^2;\ B_{44} = -\frac{1}{2}\left[\frac{1}{Sc}\mathbf{D}^2 + d_{1,r}^{n+\frac{1}{2}}\mathbf{D}\right] - \frac{d_{5,r}^{n+\frac{1}{2}}}{\Delta\xi};$$

$$K_1 = -a_{4,r}^{n+\frac{1}{2}};\ K_2 = -b_{5,r}^{n+\frac{1}{2}};\ K_3 = -c_{5,r}^{n+\frac{1}{2}};\ K_4 = -d_{4,r}^{n+\frac{1}{2}}.$$

The collocation points $N_x = 100$ are used in this study for all cases. Noticed that the SQLM depends on the value of any quantity computation, suppose F_{r+1}^{n+1} at each time step. This is attained by iterating using the QLM. The iteration calculations are carried until some appropriate tolerance level, ϵ_1, is attained. The tolerance level is stated as the maximum values of the infinity norm of the difference between the values of the calculated quantities, that is

$$max\{\|f'^{1^{n+1}}_{r+1} - f'^{1^{n}}_{r+1}\|_\infty,\ \|g^{n+1}_{r+1} - g^{n}_{r+1}\|_\infty,\ \|\theta^{n+1}_{r+1} - \theta^{n}_{r+1}\|_\infty,\ \|\phi^{n+1}_{r+1} - \phi^{n}_{r+1}\|_\infty\} < \epsilon_1 \tag{25}$$

An adequately small step size $\Delta\xi$ is considered to ensure the results accuracy.

5 Results and Discussion

The resulting nonlinear, non-homogeneous coupled partial differential equations (10)–(13) together with the boundary conditions (14) have been solved numerically using spectral quasilinearisation method. To analyze the effects of Soret, coupling number, viscous dissipation and Biot number the computations are executed for $Re_{x_0} = 200$, $Da = 0.5$, $Pr = 0.72$, $\epsilon = 0.6$, $Sc = 0.22$, and $n = 0$. In order to test the validity of code generated the existing problem numerical scheme at $\xi = 0$, has been compared with the results attained by Lloyd and Sparrow [25], Ramreddy and Pradeepa [26] for $Bi \to \infty$, $Sr = 0$, $\mathcal{B} = 0$, $N = 0$, $Da \to \infty$, $\varepsilon = 0$, $Fs = 0$ and $\lambda = 0$. The results are shown in Table 1, and the agreement is good.

Figure 2 illustrates the variation of Forchheimer number and viscous dissipation on dimensionless skin friction $\left(C_f Re_x^{1/2}\right)$, wall couple stress$(M_w Re_x)$, Nusselt number $\left(Nu_x/Re_x^{1/2}\right)$ and Sherwood number $\left(Sh_x/Re_x^{1/2}\right)$ against streamwise coordinate (ξ). Figure 2 exhibits that as viscous dissipation parameter rises the skin friction and mass transfer rate enhances, wall couple stress and heat transfer rate diminish for both Darcian ($Fs = 0.0$) and non-Darcian flows ($Fs = 0.5$). Moreover, it is observed that the skin friction, heat, and mass transfer rates are lower but wall couple stress is higher for Darcian flow compared with that of non-Darcian flow. For both Darcian and non-Darcian flow, there is no significant effect on the skin friction, wall couple stress, and heat transfer rate but mass transfer rate increases slightly in the case of vertical plate ($\xi = 0$), whereas in truncated cone ($\xi > 0$) skin friction and mass transfer rate

Table 1 Comparison analysis of $-\theta'(0, 0)$ with the proposed method(SQLM) and that of results obtained by Lloyd and Sparrow [25]

Pr		$-\theta'(0, 0)$	
Pr	Lloyd and Sparrow [25]	Ramreddy and Pradeepa [26]	Present
0.003	0.02937	0.03967	0.03967
0.01	0.0515	0.05382	0.05382
0.03	0.08439	0.08443	0.08443
0.72	0.2956	0.29564	0.29564
10	0.7281	0.72814	0.72814
100	1.572	1.57184	1.57184

Ramreddy and Pradeepa [26] when $n = 0.0$, $\varepsilon = 0$, $\mathcal{B} = 0$, $Da \to \infty$, $N = 0$, $\epsilon = 1$, $Da \to \infty$, $Bi \to \infty$, $\xi = 0$, $Sr = 0$, $Fs = 0$ and $\lambda = 0$

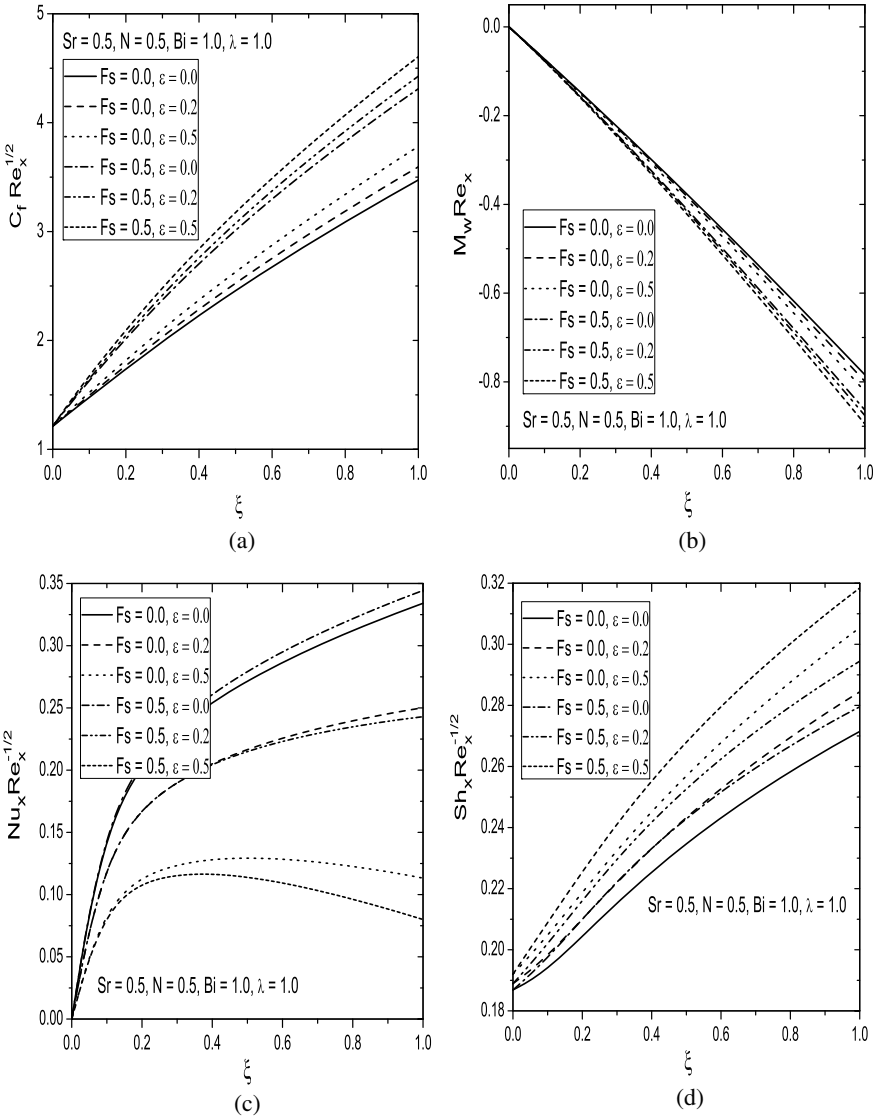

Fig. 2 Effect of *Fs* and ε on **a** skin friction **b** wall couple stress **c** Nusselt number and **d** Sherwood number

raises, but wall couple stress and Nusselt number diminishes with increase of viscous dissipation parameter.

The influence of Biot and Soret numbers on dimensionless skin friction $\left(C_f Re_x^{1/2}\right)$, wall couple stress$(M_w Re_x)$, Nusselt number $\left(Nu_x/Re_x^{1/2}\right)$, and Sherwood number $\left(Sh_x/Re_x^{1/2}\right)$ is depicted in Fig. 3. The diffusion of mass due to the temperature

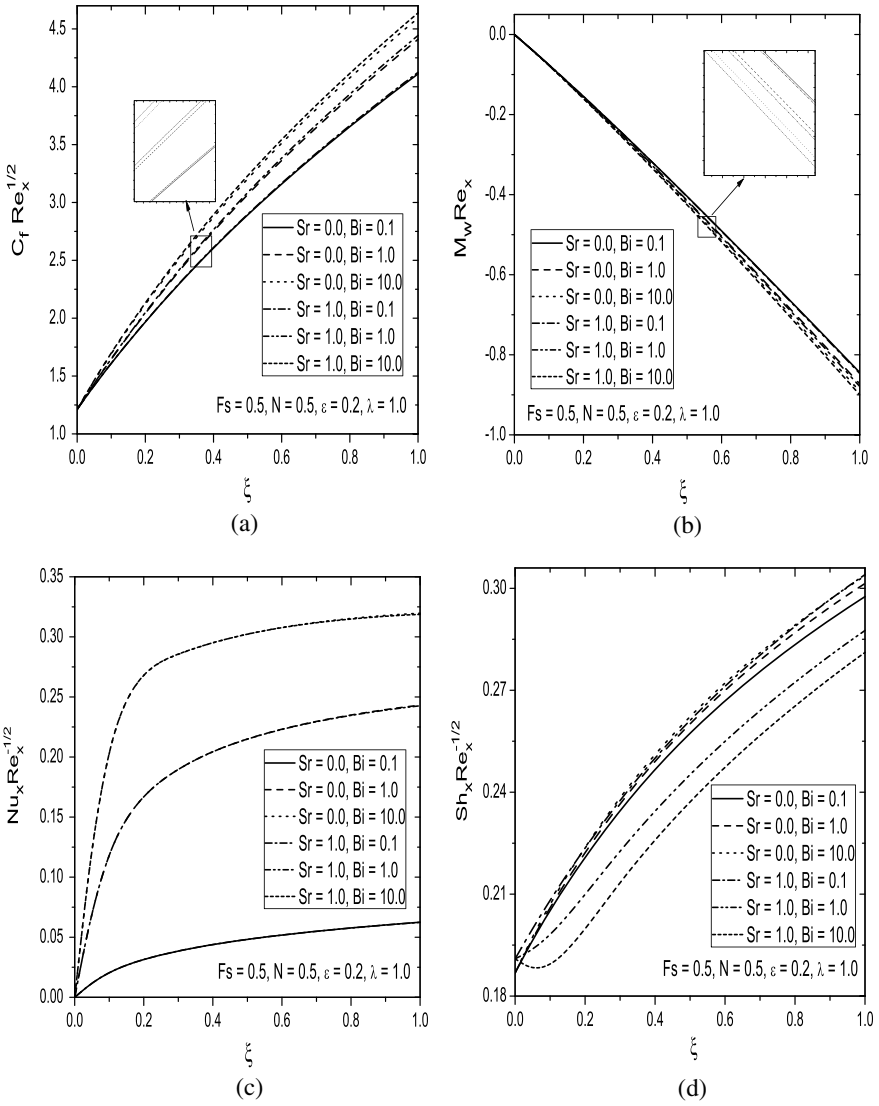

Fig. 3 Effect of *Sr* and *Bi* on **a** skin friction **b** wall couple stress **c** Nusselt number and **d** Sherwood number

gradients is delineated as Soret number *Sr*. Figures 3a, b display that for both absence($Sr = 0.0$) and presence($Sr = 1.0$) of Soret number, the wall couple stress diminishes, and skin friction enhances with the raise of Biot number. Figure 3c displays that for both the presence and absence of Soret number, the $\left(Nu_x/Re_x^{1/2}\right)$ augments nonlinearly with an increase of Biot number, but there is no immense effect with rise in Soret number. While raising the Biot number the $\left(Sh_x/Re_x^{1/2}\right)$ enhances

in the absence of Soret number $Sr = 0.0$, and with an existence of Soret number $Sr = 1.0$, it diminishes which is shown in Fig. 3d.

The dimensionless skin friction $\left(C_f Re_x^{1/2}\right)$, wall couple stress $(M_w Re_x)$, Nusselt number $\left(Nu_x/Re_x^{1/2}\right)$, and Sherwood number $\left(Sh_x/Re_x^{1/2}\right)$ with mixed convection parameter variation for both micropolar $(N = 0.5)$ viscous fluids $(N = 0)$ is shown in Fig. 4. The coupling number(N) characterizes the rotational and linear motion of fluid particles. Figure 4a illustrates that for both $(N = 0)$ and $(N = 0.5)$ the skin friction in opposing flow case is low and in aiding flow is more as compared with forced convection flow. Further noticed that the skin friction is high in case of micropolar fluid than compared with that of viscous fluid case because micropolar fluid offers high resistance which emerge from fluid particles motion. Figure 4b portrays that for micropolar fluid the wall couple stress is less in case of aiding flow than that of opposing flow case. Figures 4c, d represent that the heat and mass transfer rates of micropolar fluid are lower than that of viscous fluid. Moreover, for both fluids $(N = 0.0$ and $N = 0.5)$, the $\left(Nu_x/Re_x^{1/2}\right)$ and $\left(Sh_x/Re_x^{1/2}\right)$ are less in case of opposing flow as compared with forced convection and aiding flow.

Figure 5 portrays the effect of material constant parameter and porosity on dimensionless skin friction$\left(C_f Re_x^{1/2}\right)$, wall couple stress$(M_w Re_x)$, Nusselt number $\left(Nu_x/Re_x^{1/2}\right)$, and Sherwood number $\left(Sh_x/Re_x^{1/2}\right)$ against streamwise coordinate (ξ). Figure 5a exhibits that the skin friction decreases and then increases with increase of porosity. The skin friction decreases with increase of material constant parameter. The wall couple stress enhances with the enhancement of both ϵ and n displayed in Fig. 5b. Figure 5c shows that Nusselt number increases and decreases with increase of ϵ and n, respectively. As the porosity increases the Sherwood number decreases first and then increases which is clearly observed in Fig. 5d. Moreover, Sherwood number increases with increase of material constant parameter.

6 Conclusions

A mathematical model of steady mixed convection incompressible micropolar fluid flow over a truncated cone embedded in a saturated porous medium with viscous dissipation and thermal diffusion effects is investigated in this paper. In addition, Forchheimer porous medium with convective boundary condition is incorporated. The resulting non-similarity equations are solved using spectral quasilinearization method. Based on the analysis carried out, the main conclusions are drawn

- For both presence $(Fs = 0.5)$ and absence $(Fs = 0.0)$ of Forchheimer number, the Sherwood number and skin friction increases, whereas wall couple stress decreases with raise in viscous dissipation.

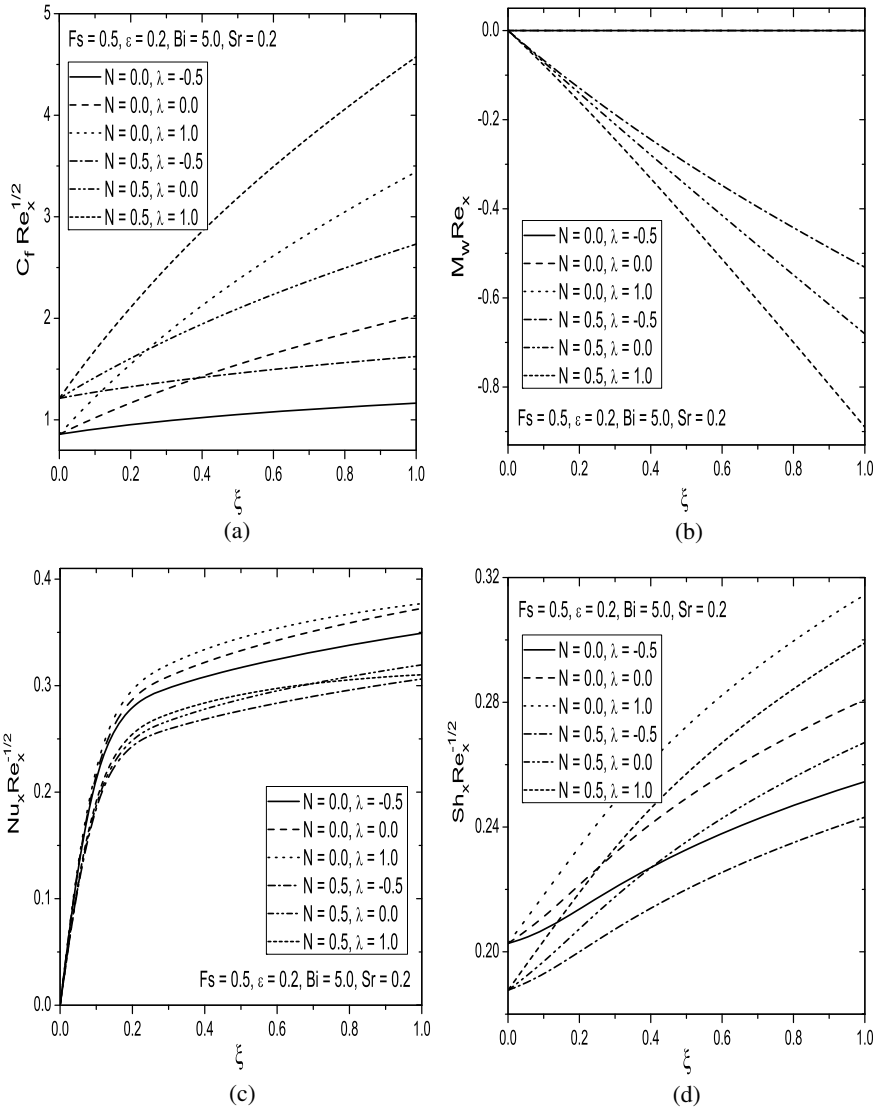

Fig. 4 Effect of N and λ on **a** skin friction **b** wall couple stress **c** Nusselt number and **d** Sherwood number

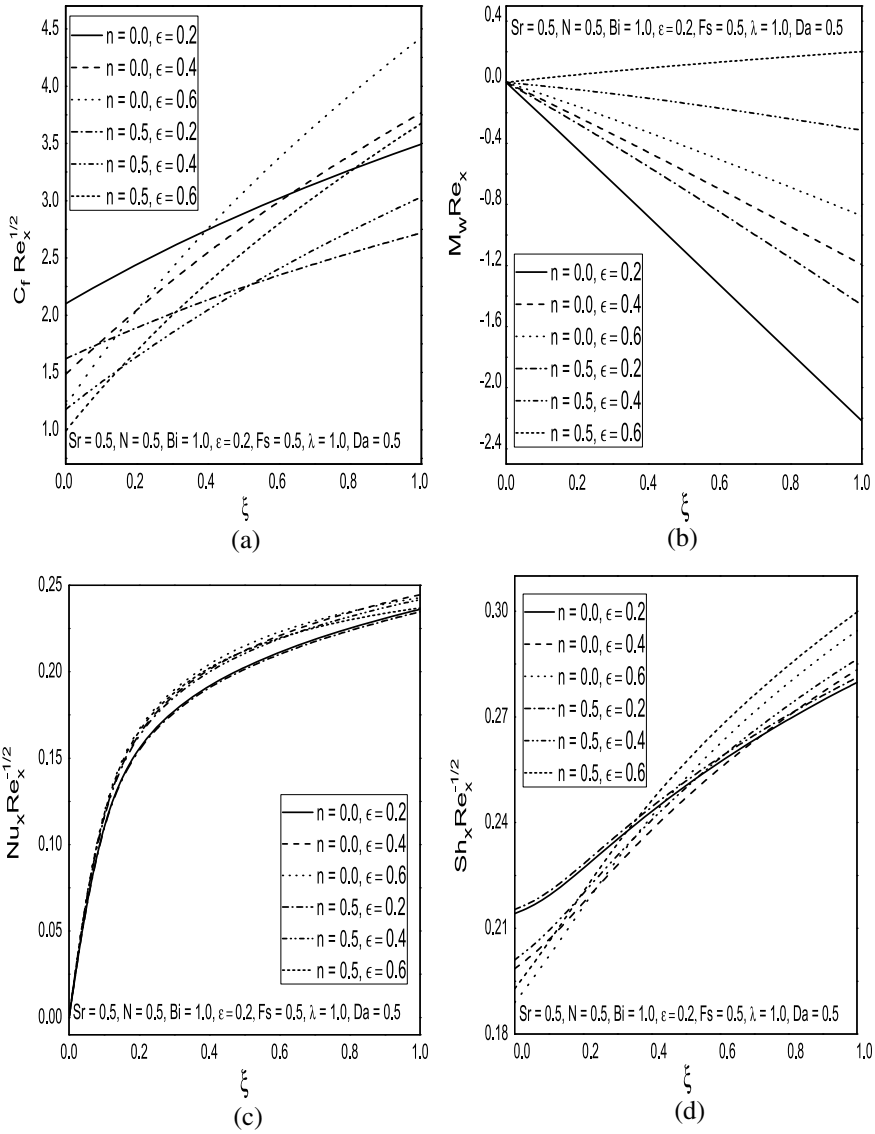

Fig. 5 Effect of n and ϵ on **a** skin friction **b** wall couple stress **c** Nusselt number and **d** Sherwood number

- The raise in Biot number results to diminish the wall couple stress, but raises Nusselt number, skin friction for both the cases, i.e., presence and absence of Soret number. Meanwhile, as the Biot number increases, the Sherwood number shows the opposite behavior for the cases of $Sr = 0.0$ and $Sr = 1.0$.
- In the opposing flow, the Sherwood number and skin friction are more for both viscous and micropolar fluids. The Nusselt number is less for opposing flow as compared with forced convection and aiding flow.
- The skin friction and Sherwood number show similar behavior with increase of porosity, but they show opposite behavior with increase of material constant parameter. The wall couple stress and Nusselt number increases with increase of porosity; however, they show opposite behavior with increase of material constant parameter.

References

1. Ingham DB, Pop I (2005) Transport phenomena in porous media. Elsevier, Oxford
2. Nield DA, Bejan A (2013) Convection in porous media, 4th edn. Springer, New York
3. Vafai K (2015) Handbook of porous media, 3rd edn. CRC Press, Taylor and Francis Group
4. Eringen AC (1966) Theory of micropolar fluids. J Math Mech 16:1–18
5. Ariman T, Turk MA, Sylvester ND (1973) Microcontinuum fluid mechanics—a review. Int J Eng Sci 11(8):905–930
6. Ariman T, Turk MA, Sylvester ND (1974) Applications of microcontinuum fluid mechanics. Int J Eng Sci 12(4):273–293
7. Lukaszewicz G (1999) Micropolar fluids—theory and applications. Birkhauser, Basel
8. Eremeyev V, Lebedev L, Altenbach H (2013) Foundations of micropolar mechanics. Springer, New York, Heidelberg
9. Gebhart B (1962) Effect of viscous dissipation in natural convection. J Fluid Mech 14:225–235
10. El-Amin MF, Mohammadein AA (2005) Effects of viscous dissipation and Joule heating on magnetohydrodynamic Hiemenz flow of a micropolar fluid. Heat Transf Eng 26(6):75–81
11. El-Aziz MA (2009) Viscous dissipation effect on mixed convection flow of a micropolar fluid over an exponentially stretching sheet. Canadian J Phys 87(4):359–368
12. Ahmad K, Ishak A, Nazar R (2013) Micropolar fluid flow and heat transfer over a nonlinearly stretching plate with viscous dissipation. Math Problems Eng 2013:1–5
13. Yih KA (1999) Coupled heat and mass transfer by free convection over a truncated cone in porous media: VWT/VWC or VHF/VMF. Acta Mechanica 137(1–2):83–97
14. Cheng CY (2012) Natural convection boundary layer flow over a truncated cone in a porous medium saturated by a nanofluid. Int Commun Heat Mass Transf 39:231–235
15. Postelnicu A (2012) Free convection from a truncated cone subject to constant wall heat flux in a micropolar fluid. Meccanica 47:1349–1357
16. Patrulescu FO, Groşan T, Pop I (2014) Mixed convection boundary layer flow from a vertical truncated cone in a nanofluid. Int J Numerical Methods Heat Fluid Flow 24(5):1175–1190
17. Srinivasacharya D, Ramreddy Ch (2012) Mixed convection in a doubly stratified micropolar fluid saturated non-Darcy porous medium. Canadian J Chem Eng 90(5):1311–1322
18. Ahmadi G (1976) Self-similar solution of incompressible micropolar boundary layer flow over a semi-infinite plate. Int J Eng Sci 14:639–646
19. Cowin SC (1968) Polar fluids. Phys Fluids 11:1919–1927
20. Srinivasacharya D, Motsa SS, Surender O (2015) Numerical study of free convection in a doubly stratified non-Darcy porous medium using spectral quasilinearization method. Int J Nonlinear Sci Numerical Simul 16:173–183

21. RamReddy C, Pradeepa T (2016) Non-similarity solution of micropolar fluid flow over a truncated cone with Soret and viscous dissipation effects using spectral quasilinearization method. Int J Appl Comput Math 1–15. https://doi.org/10.1007/s40819-016-0227-y
22. Bellman RE, Kalaba RE (1965) Quasilinearisation and non-linear boundary-value problems. Elsevier, New York
23. Trefethen LN (2000) Spectral methods in MATLAB. SIAM
24. Canuto C, Hussaini MY, Quarteroni A, Zang TA (2006) Spectral methods fundamentals in single domains. Springer, New York
25. Lloyd JR, Sparrow EM (1970) Combined free and forced convective flow on vertical surfaces. Int J Heat Mass Transfer 13:434–438
26. Ramreddy C, Pradeepa T (2017) Non-similarity solutions for viscous dissipation and Soret effects in micropolar fluid over a truncated cone with convective boundary condition: spectral quasilinearization approach. Int J Nonlinear Sci Numerical Simul 18(5):327–342